



Effects of wind and choice of cover material on the yield of a passive solar still

J. Andrew Jones, Laura W. Lackey*, Kevin E. Lindsay

*Department of Environmental Engineering, Mercer University, Macon, GA 31207, US
Tel. +1 478 301 4106; Fax: +1 478 301 2331; email: lackey_l@mercer.edu*

Received 19 December 2012; Accepted 7 March 2013

ABSTRACT

The development of an accurate thermodynamic model for the basic solar still has been the goal of many researchers. Glass covers are the most common choice of cover material, but are not always available under all situations and pose a large risk of physical injury if not handled with precaution. The effects of using three different cover materials (glass, Plexiglas, and plastic wrap) were investigated under a series of environmental conditions. The heat transfer model has been improved upon by the incorporation of a term for the effective emissivity of the cover, τ_{eff} . The effective τ expands upon the definition of the basic τ by incorporating the reflecting effects of the condensed, but not yet collected, water droplets adhered to the interior surface of the cover. The cumulative yield and water temperature profile predictions of the improved model were verified by a comparison with experimental results.

Keywords: Solar distillation; Tau effective; Solar still; Desalination; Wind effects

1. Introduction and background

Ninety-seven percent of the world's available water supply is unfit for human consumption due to its large salt concentration [1]. Multitudes of people around the world suffer from severe water shortages and available potable water sources are becoming a desirable commodity. A procedure known as desalination, removing salts from water, has gained much attention in the literature as a solution to the problem. Large-scale desalination systems are used in many countries around the world, most notably in India and the Middle East where the arid climate causes the production of freshwater to be a necessity [1]. A compact, lightweight solar distillation unit would be beneficial

in the immediate aftermath of a natural disaster to provide short-term relief.

The literature is flooded with different designs and configurations for solar distillation (SD) apparatus, many of which contain mathematical models and simulations predicting maximum efficiency. Several excellent reviews have been recently published [2–6]. Reviews specific to active [7] and passive solar distillation [8] are also available. Many investigators have summarized and modeled results for specific locations [9]. All types of SD units exhibit similar problems such as low yields and large surface area to yield ratios.

The components of a single-slope, basin-type SD units are shown in Fig. 1 and consist of: (1) an absorptive plate or black surface, (2) water layer, (3) insula-

*Corresponding author.

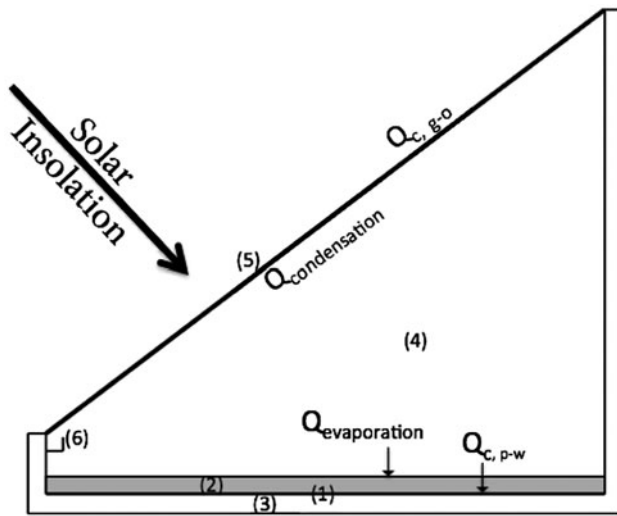


Fig. 1. The basic solar still design with labeled components and energy transfers. (1) absorptive plate, (2) seawater, (3) insulation, (4) humid air, (5) glass cover, (6) collection trough.

tion, (4) humid air, (5) glass cover, and (6) collection trough.

A single-slope solar still as shown in Fig. 1 is comprised of an insulated box with the top cover made from a material with high transmittance and thermal conductance (most commonly glass). There are three main areas of a simple solar still including: the insulated sides, the absorptive basin to hold seawater, and the cover. The sides of the container are insulated to decrease heat loss from the brine solution through the sides of the apparatus. The basin serves two functions: to hold the seawater and to absorb light energy passing through the seawater before it is lost to the environment. To maximize absorption, the sides and bottom of the container are commonly black. The cover is also multipurpose—it seals the system from any mass transport to the system surroundings, while still allowing energy in the form of direct thermal insolation to enter. It also serves as the condensation surface to collect the freshwater output. The collection of thermal radiation inside the device will cause the interior temperature to rise causing an increase in the vapor pressure of water in the solution. When the hot water vapor hits the relatively cool cover, the water vapor will condense, form droplets, and with help from gravity, roll down the inclined plane to be collected in a bottle or trough. Refer to area (6) of Fig. 1 for a visual representation of the condensate collection trough.

The goal of this project was to design, build, test, and mathematically model a single-slope SD unit

fitted with three unique cover materials including plastic wrap, that would typically be found in a kitchen cabinet, glass, and Plexiglas. The effects of the different covers on the temperature and the yield of the system were analyzed and explained with the heat transfer model.

2. Heat transfer modeling equations

Energy balances are performed on primary still components including the absorptive plate, the water in the absorptive basin, the humid air, and for the transparent cover. A differential energy balance around the absorptive plate, as shown in Eq. (1), was used to determine the temperature of the plate (T_p). It was assumed that the absorptive plate absorbed all solar insolation and the heat transfer due to radiation was insignificant when compared to that of convection.

$$\Delta E = M_p C_p \frac{dT_p}{dt} = \text{Solar radiation} - Q_{c,p-w} - Q_{p-o} \quad (1)$$

The solar insolation was calculated as

$$\text{Solar radiation} = I\alpha\tau \quad (2)$$

where, I represents the total incoming solar insolation, τ accounts for the losses due to cover emissivity, and α accounts for the losses due to the absorptivity of the plate. Eq. (3) shows Newton’s Law of Cooling that describes the heat transfer by convection from the plate to the water. The thermal resistance model as shown in Eq. (4) describes the transfer of energy from the plate to the environment.

$$Q_{c,p-w} = h_{c,p-w}(T_p - T_w) \quad (3)$$

$$Q_{p-o} = \frac{(T_p - T_o)}{\frac{L_p}{K_p} + \frac{L_l}{K_l} + \frac{1}{h_{c,l-o}}} \quad (4)$$

Substitution of Eqs. (2)–(4) into the energy balance for the adsorptive plate yields

$$M_p C_p \frac{dT_p}{dt} = I\alpha\tau - h_{c,p-w}(T_p - T_w) - \frac{(T_p - T_o)}{\frac{L_p}{K_p} + \frac{L_l}{K_l} + \frac{1}{h_{c,l-o}}} \quad (5)$$

Two modes of energy transfer were considered to determine T_w . It was assumed that the only heat introduced to the water was from convective heat transfer

from the absorptive plate, as shown in Eq. (3), and energy was lost due to evaporation ($Q_{\text{evaporation}}$).

$$\Delta E = \rho_w C_w b \frac{dT_w}{dt} = Q_{c,p-w} - Q_{\text{evaporation}} \quad (6)$$

The energy lost due to evaporation was estimated using the semi-empirical term called the Ryan Correlation [10]. The correlation, from Ryan (1974), is based on measurements in open water bodies (e.g. lakes and ponds) and implements a velocity term to represent the wind speed in meters per second across the fluid surface [10]. Neglecting the wind term in the Ryan Correlation results in Eq. (7) for estimating the heat loss from evaporation in the SD unit.

$$Q_{\text{evaporation}} = 0.027(T_w - T_A)^{1/3} P_{\text{SAT}}(1 - H_R) \quad (7)$$

Substituting Eqs. (3) and (7) into Eq. (6) provides the expression used to determine the differential temperature of the water.

$$\rho_w C_w b \frac{dT_w}{dt} = h_{c,p-w}(T_p - T_w) - 0.027(T_w - T_A)^{1/3} P_{\text{SAT}}(1 - H_R) \quad (8)$$

The energy transfer for the humid air domain is shown as Eq. (9).

$$\Delta E_{\text{humid air}} = \rho_A C_A L_A \frac{dT_A}{dt} = Q_{\text{evaporation}} - Q_{\text{condensation}} \quad (9)$$

The evaporative heat flux into the air was again modeled using the Ryan Correlation as shown in Eq. (7). The heat flux from the air domain is due to the condensation of water and is represented by another semi-empirical formula (Eq. (10))[11].

$$Q_{\text{condensation}} = 85.0(T_A - T_G)H_R \quad (10)$$

Substituting Eqs. (7) and (10) into Eq. (9) results in the governing equation used to model heat transfer in the humid air domain.

$$\rho_A C_A L_A \frac{dT_A}{dt} = 0.027(T_w - T_A)^{1/3} P_{\text{SAT}}(1 - H_R) - 85.0(T_A - T_G)H_R \quad (11)$$

The energy balance for the cover is presented as Eq. (12).

$$\Delta E = M_G C_G \frac{dT_G}{dt} = Q_{\text{condensation}} - Q_{c,g-o} \quad (12)$$

Substituting into Eq. (12), results in Eq. (13) representing the energy balance for the cover domain.

$$M_G C_G \frac{dT_G}{dt} = 85.0(T_A - T_G)H_R - h_{c,g-o}(T_G - T_o) \quad (13)$$

3. Modeling mass transfer

The still is assumed to be a closed system, so no mass is transferred into or out of the SD unit boundary. The phase change at the water surface results in an evaporative mass flux that increases the partial pressure of water in the air–vapor mixture. To predict yield, the condensation flux occurring at the air–vapor mixture and cover boundary was considered. A straightforward relationship [11] as shown in Eq. (14) links the condensation heat transfer and mass condensation rate.

$$\begin{aligned} \frac{dm_{\text{condensation}}}{dt} &= \frac{Q_{\text{condensation}}}{\text{Latent heat of vaporization}} \\ &= \frac{85.0(T_A - T_G)H_R}{h_{fg}} \end{aligned} \quad (14)$$

The rate of condensation, having units of kg/s m^2 , is determined. Integration over the duration of the SD unit operation results in the total mass of condensate produced per unit area of the still cover (kg/m^2). It is assumed that all condensate is collected with 100% efficiency and none is returned to the water basin.

4. Experimental setup

Three solar stills were constructed from locally available Styrofoam coolers; the wall thickness of the coolers was 4 cm. The dimensions of the completed solar stills were: Height—40 cm, Length—83 cm, and Width—40 cm. The most effective cover angle has been well researched and has led to conflicting results. A recent excellent review [12] was published on this conflict. The cover angle of 45° was chosen to maximize cover surface area while minimizing the effect of water droplets dripping back into the basin [13]. The interior of the stills was painted flat black and a 10-cm layer of black aquarium rock (average diameter—6 mm) was placed in the basin to act as the absorptive plate. The water collection trough consisted of a modified one-half inch CPVC pipe, cut in half lengthwise, and secured to the SD unit housing with clear silicone adhesive. The collection trough was connected to the external collection bottle with commonly available CPVC and PVC fittings. The covers were applied to the angled surface of the solar still using

clear silicone adhesive. Three cover materials were evaluated in this study: glass (thickness=2.4 mm), Plexiglas (thickness=3 mm), and clear polyethylene plastic wrap (thickness=0.05 mm).

At the onset of each experimental run, the solar stills were loaded with 2 liters of tap water through an access plug, cut in the back wall of the cooler. This access plug was then sealed with silicone to reduce leaks to the surroundings.

The temperature of water in the basin was measured using a LM35 Precision centigrade temperature sensor. The sensor supplied a linear temperature response at a slope of 10 mV/°C with an accuracy of $\pm 0.5^\circ\text{C}$. The exposed wires and the LM35 package were coated with silicone for waterproofing. The connecting wires for the temperature sensor were run through the rear access plug and placed directly in the water layer. Solar insolation was measured using a Fisher Scientific Traceable Handheld Digital Light Meter with analog output. Insolation was measured on the same angle and plane as the solar still covers. The light meter has a specified accuracy of $\pm 5\%$ over the range measured.

The temperature and solar insolation data were recorded using the NI USB-6008 analog to digital converter and LabVIEW software. The entire SD system was manually rotated approximately every hour during testing to follow the sun. Effluent yields were manually measured.

5. Results and discussion

The mass and heat transfer equations were solved using Berkeley Madonna, an ordinary differential equations software package designed at the University of California at Berkeley. Material properties, heat transfer coefficients, and system dimensions were coded into Berkeley Madonna. Empirical relationships were used to represent properties that change with system temperatures (water vapor pressure, water density, and air density) or those that were specific to the testing day (i.e. ambient temperature and solar intensity). The depth of water in the basin, b , decreased with run time and was modeled as a function of water condensed and collected.

An effective emissivity of the covers, τ_{eff} , was measured using the solar meter to record solar readings from the exterior and interior of the solar still. The fraction of light passing through the cover was taken to be τ_{eff} . τ_{eff} represents the emissivity of the respective cover materials as well as the fraction of sunlight reflected by the water droplets condensed on the cover that have not yet been collected. The τ_{eff} values

were observed to vary throughout the day, quickly decreasing a couple hours after sunrise, leveling out during the middle of the day, and rising back to their original level after sunset. The extent of the rise and fall for τ_{eff} varied for the three different cover materials and the τ_{eff} profiles are shown in Fig. 2.

The measured τ_{eff} profiles were integrated into the model to account for the subsequent decrease in effective insolation available to heat the system.

Water temperature and yield were measured for three different cover materials (glass (G), Plexiglas (PG), and clear polyethylene plastic wrap (PW)). The data were collected on sunny, clear, precipitation-free days; the solar intensity peaked between 1,000 and 1,200 W/m² on each day and followed a smooth non-skewed parabolic path. The winds were calm through the early part of the day, but picked up toward the early evening. The water temperature profiles were similar in shape for all three solar stills but the maximum temperature was generally higher for G than PG (approx. 2°C), and for PG than PW (approx. 8°C). The output yield of the three systems was highest for the G cover, followed by the PW, and then the PG.

During a typical testing day, the solar stills displayed quick heating during the morning reaching their equilibrium temperature around midday. The rate of freshwater production from the stills was very slow during the morning hours but picked up quickly during the hours of maximum solar insolation immediately preceding midday. Figs. 3 and 4 contain data from a single typical day (5 October). Fig. 3 displays the solar insolation profile (left axis) and the cumulative yield (right axis) vs. time of day. The sunrise can be observed at 7:30 and the sunset at 19:10 from the solar insolation values. Notice that the freshwater production rates in the morning hours and after sunset are small compared to the midday production rates.

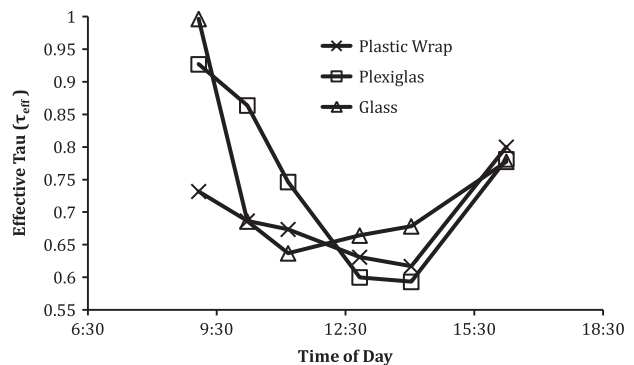


Fig. 2. The change of τ_{eff} over the course of the testing day.

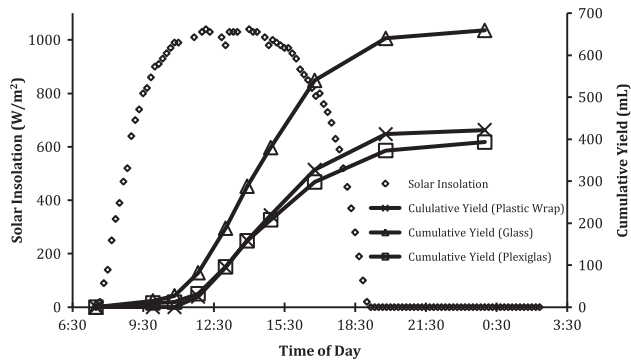


Fig. 3. Typical daily relationship between solar insolation and cumulative yield for all three cover materials.

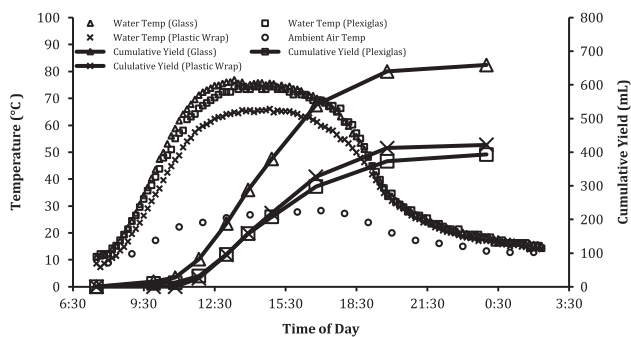


Fig. 4. Typical water temperature, ambient air temperature, and cumulative yield vs. time for all cover materials.

Production between 12:00 and 16:00 accounted for approximately 70% of the cumulative yield.

A similar trend was also seen between the typical water temperature and cumulative freshwater yield. Fig. 4 shows the similar correlation that approximately 70% of the total yield was obtained when the temperature of the water was above 60°C, which also corresponds to the time of day from noon to 16:00.

Interestingly, as shown in Fig. 4, higher internal water temperature does not directly correlate to higher cumulative yields regardless of cover material. The Plexiglas SD unit displays a higher water temperature but a lower yield as compared to the plastic wrap SD unit. This phenomenon is predicted to be due to the larger effects of small mechanical interactions (i.e. wind, vibrations, etc.) on the less rigid plastic wrap cover. Further investigation into the adhesion of water to the cover surface under a variety of perturbations is needed to fully understand this phenomenon.

The trends shown in Figs. 3 and 4 are commonly observed [14–16]. Table 1 summarizes measured data for all cover materials and climatic conditions for multiple days of data collection. The day 5 October

2011 was used in the comparisons to the thermodynamic model. Thermal and exergy efficiencies were also calculated for the three solar stills as presented by Tiwari et al. [17], and are presented in Table 2.

The effects of wind (sustained and gusts) on the solar still were not incorporated into the thermodynamic model. Wind affects the solar still by increasing the heat transfer from the cover to the outside ambient air due to forced convection [18] and by forcing micro movement of the cover giving the condensed, but not yet collected, water droplets sufficient energy to overcome contact angle hysteresis [19] and slide down the cover to the collection trough. At low sustained speeds, the wind was shown to increase the output of the solar still up to a point where a further increase in wind speed was then detrimental to the yield due to excessive movement of the cover such that droplets adhered to the cover surface were disturbed and fell from the cover back to the water reservoir without being collected. This correlation is shown in Fig. 5. The data were fitted with a second-order polynomial to represent the phenomena described above. The days represented in Fig. 5 were selected to minimize the effects of other (non-wind) parameters on yield. The small differences in climatic conditions for the testing days are described in Table 1.

The effect of wind speed on solar distillation production is controversial. A variety of researchers have shown that an increase in wind speed increases production [14,20–23], while others have shown increased wind speeds to cause a decrease in productivity [24–27]. Recent theoretical modeling performed by El-Sebaï indicate that in single-incline passive solar still, there is a critical mass (or depth) of basin water beyond which the productivity increases with the increase in wind speed, up to some critical wind speed. For SD basins containing less than the critical mass of water, an increase in wind speed causes a decrease in productivity. If the critical wind speed is realized or exceeded, it is predicted to have minimal influence on production [28,29]. As described by El-Sebaï (2004), the critical mass density of basin water was shown to be 45 kg H₂O/m² of plate surface area. The relative initial condition for our work was 11 kg H₂O/m² of plate surface area. We observed an increase in production when wind speeds were generally less than 1 m/s, suggesting that system variables other than critical depth influence wind-speed impact on production.

Comparing the modeling results with the experimental data showed the efficacy of the thermodynamic model. Experimental data were taken regarding yield and internal water temperature of solar stills with the

Table 1
Summary of measured data and climatic conditions for all testing days

Date	Cover material	Max water temperature (°C)	Yield (mL)	Max solar insolation (W/m ²)	Ave. wind speed (m/s) ^a	Max/Min ambient temperature (°C) ^a	Weather ^a
10/5/11	Glass	76.9	659				
	Plexiglas	74.4	393	1,040	0.72	29/6	Sunny
	Plastic Wrap	66.1	422				
10/6/11	Glass	69.3	621				
	Plexiglas	68.3	390	1,050	1.23	29/9	Sunny
	Plastic Wrap	61.0	424				
3/17/11	Glass	75.8	668				
	Plexiglas	67.7	367.5	1,240	1.23	25/2	Sunny
	Plastic Wrap	65.8	340				
3/18/11	Plexiglas	64.9	489	1,250	0.21	29/3	Partially Cloudy
	Plastic Wrap	68.3	325				
3/23/11	Glass	64.0	293				
	Plexiglas	62.1	245	1,377	2.00	29/11	Cloudy
	Plastic Wrap	57.4	142				

^aData obtained from almanac archives.

Table 2
Thermal energy and exergy efficiencies for three solar still cover types

Cover material	Thermal efficiency (%)	Exergy efficiency (%)
Glass	25.1 ± 2.3	3.6 ± 0.3
Plexiglas	14.9 ± 2.2	3.4 ± 0.4
Plastic wrap	15.5 ± 3.4	3.0 ± 0.2

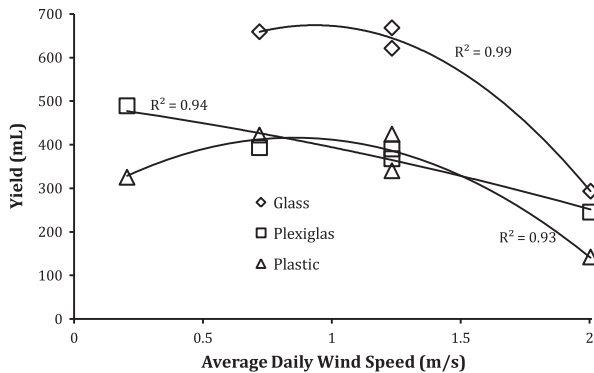


Fig. 5. Relationship between the average daily wind speed and the yield of a solar distillation device. Second-order lines of best fit are shown with associated R2 values.

three different cover materials. Fig. 6 presents the cumulative freshwater yields vs. time, where the lines indicate modeling predictions and the markers indicate experimental data points. A statistical analysis of the data indicates the modeling results fit ($R^2 > 0.9$, NRMS

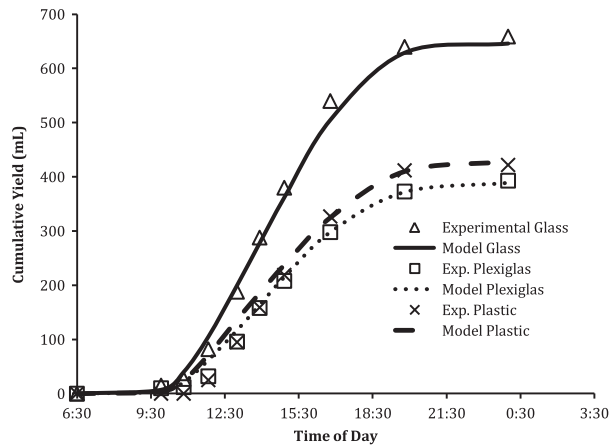


Fig. 6. Efficacy of the model for predicting freshwater yield.

error < 5.6%) the experimental temperature and yield profiles. The R^2 values and normalized RMS error calculations for the aforementioned correlations have been presented on the appropriate figures below.

A comparison was done with the experimental data collected for three cover types on 5 October. Normalized RMS errors for glass, Plexiglas, and plastic wrap were found to be 2.6, 3.2, and 5.6%, respectively.

Temperature data from the same day was also compared with the modeling results. The results seen in Figs. 7–9 show a good fit for the data through the morning and afternoon.

After sunset, the theoretically predicted temperature profiles digress from the observed experimental

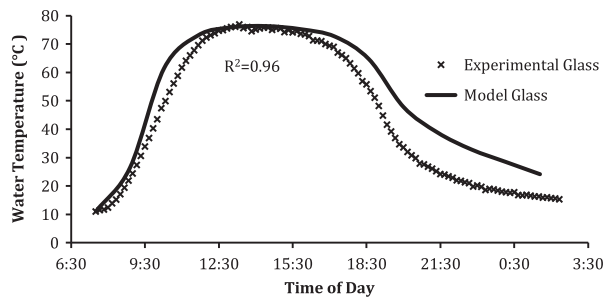


Fig. 7. Modeling and experimental comparison of water temperature profiles for a solar still with a glass cover. Normalized RMS error calculated to be 13.2%.

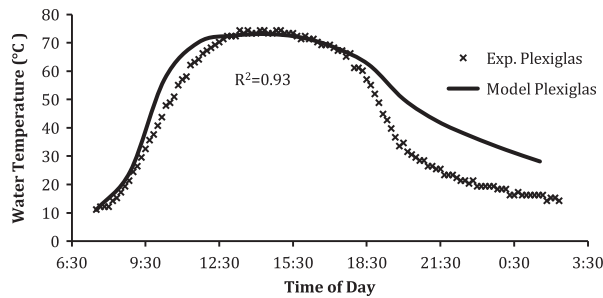


Fig. 8. Modeling and experimental comparison of water temperature profiles for a solar still with a Plexiglas cover. Normalized RMS error calculated to be 15.3%.

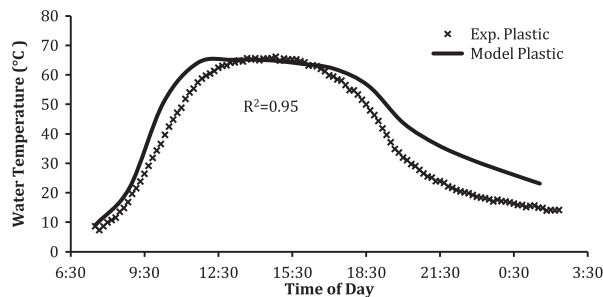


Fig. 9. Modeling and experimental comparison of water temperature profiles for a solar still with a plastic wrap cover. Normalized RMS error calculated to be 13.9%.

temperatures, decreasing at a much greater rate than those predicted by the model. Forced convection across the cover due to windy afternoon conditions provides a plausible explanation for the observed increase in cooling rate. Almanac data from the testing date indicate that the wind speeds were elevated from 14:00 until 18:00. Fig. 10 shows the graph of wind speed almanac data for 5 October.

The substantial difference between experimental and model-predicted evening temperatures, due to the windy conditions, did not affect the yield predictions or observations. We conclude that this is from the

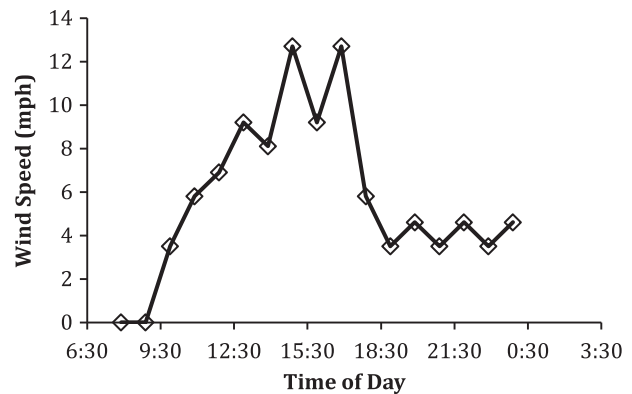


Fig. 10. Wind speed profile for 5 October.

timing of the elevated, sustained winds. The highest sustained winds appeared, beginning at 15:00 and continuing until 18:00. The hours of highest yield production occurred from 12:00 until 16:00. The small time overlap between these regions was not enough to cause a substantial change in the experimental freshwater production; therefore, resulting in theoretical and experimental yield profiles displaying higher coefficients of determination, R^2 , than as compared to the corresponding temperature profiles.

6. Conclusion

Single-slope solar distillation units equipped with three different cover materials were designed, built, and tested. Cover materials used included glass, Plexiglas, and plastic wrap. The highest internal water temperature and freshwater yield were consistently produced by the solar still fitted with a glass cover. The Plexiglas cover resulted in higher (8°C) water temperature but slightly lower (7%) freshwater yield than the solar still equipped with a plastic wrap cover. A convective heat transfer thermodynamic model for a basic solar still was developed. Good agreement between simulation and experimental results ($R^2 > 0.93$) was observed. Improvements can be made to the model by taking into account the effects of wind. These effects include: forced convection from the cover to the ambient air and the addition of kinetic energy to the water collection process. The development of a parameter for the effective emissivity of the cover, τ_{eff} , allows the model to account for the decrease in incoming solar insolation due to the reflection of sunlight by the condensed, but not yet collected, water droplets adhered to the internal surface of the cover. The general trend and expected results are all consistent between the model and experimental data, indicating the validity of the differential model.

Nomenclature and symbols

Symbol	Value	Units	Description
b	0.011 (Initially)	m	thickness of seawater
C_A	1,006	J/kg °C	specific heat capacity of humid air
C_G	840	J/kg °C	specific heat capacity of cover material
C_P	800	J/kg °C	specific heat capacity of absorption plate
C_w	4,184	J/kg °C	specific heat capacity of seawater
$h_{c,p-w}$	200	W/m ² °C	convective heat transfer coefficient from plate to water
$h_{c,i-o}$	100	W/m ² °C	convective heat transfer coefficient from insolation to ambient outside air
$h_{c,g-o}$	200	W/m ² °C	convective heat transfer coefficient from cover to outside ambient air
h_{fg}	2.4×10^6	J/kg	latent heat of vaporization for water
H_R	time variant	–	relative humidity of vapor inside the solar distillation unit
K_I	0.033	W/m ² °C	thermal conductivity of insulation
K_P	0.7	W/m ² °C	thermal conductivity of plate
L_A	0.18	m	average length between water and cover
L_I	0.038	m	length/thickness of Styrofoam insulation
L_P	0.010	m	length/thickness of absorptive plate
$m_{\text{condensation}}$	time variant	kg/m ²	mass of condensation
M_G	8.9 (glass), 6.7 (Plexiglas), 0.044 (plastic wrap)	kg/m ²	mass density of cover material
M_P	14.4	kg/m ²	mass density of absorption plate
P_{SAT}	time variant	Pa	saturated vapor pressure of water
$Q_{\text{condensation}}$	time variant	W/m ²	energy transfer due to condensation
$Q_{c,g-o}$	time variant	W/m ²	energy transfer from cover to outside ambient air
$Q_{c,p-w}$	time variant	W/m ²	energy transfer from plate to water
$Q_{\text{evaporation}}$	time variant	W/m ²	energy transfer due to evaporation
Q_{p-o}	time variant	W/m ²	energy transfer from plate to ambient outside air
t	–	s	time
T_A	time variant	°C	temperature of humid air
T_G	time variant	°C	temperature of cover material
T_O	time variant	°C	temperature of ambient outside air
T_P	time variant	°C	temperature of top of the absorption plate
T_w	time variant	°C	temperature of top of water
α	0.96	–	absorptivity of the plate
ρ_A	time variant	kg/m ³	density of humid air
ρ_w	time variant	kg/m ³	density of seawater
τ_{eff}	time variant	–	effective emissivity of the cover

References

- [1] A.D. Khawaji, I.K. Kutubkhanah, J. Wie, Advances in seawater desalination technologies, *Desalination* 221 (2008) 47–69.
- [2] E. Mathioulakis, V. Belessiotis, E. Delyannis, Desalination by using alternative energy: Review and state-of-the-art, *Desalination* 203 (2007) 346–365.
- [3] S. Kalogirou, Seawater desalination using renewable energy sources, *Prog. Energy Combust. Sci.* 31 (2005) 242–281.
- [4] A. Kaushal, Solar stills: A review, *Renew. Sustain. Energy Rev.* 14 (2010) 446–453.
- [5] G.N. Tiwari, H.P. Garg, Studies on various designs of solar distillation systems, *Solar Wind Technol.* 1 (1984) 161–165.
- [6] G.N. Tiwari, H.N. Singh, R. Tripathi, Present status of solar distillation, *Solar Energy* 75 (2003) 367–373.
- [7] K. Sampathkumar, T.V. Arjunan, P. Pitchandi, P. Senthilkumar, Active solar distillation—A detailed review, *Renew. Sustain. Energy Rev.* 14 (2010) 1503–1526.
- [8] R. Balan, J. Chandrasekaran, S. Shanmugan, B. Janarthanan, S. Kumar, Review on passive solar distillation, *Desalin. Water Treat.* 28 (2011) 217–238.
- [9] H.N. Singh, G.N. Tiwari, Monthly performance of passive and active solar stills for different Indian climatic conditions, *Desalination* 168 (2004) 145–150.
- [10] T.P. Yilmaz, H.S. Aybar, Evaluation of the correlations for predicting evaporative loss from water body, *ASHRAE Trans.* 105 (1999) 185–190.
- [11] H.Ş. Aybar, Mathematical modeling of an inclined solar water distillation system, *Desalination* 190 (2006) 63–70.

- [12] A.J.N. Khalifa, On the effect of cover tilt angle of the simple solar still on its productivity in different seasons and latitudes, *Energy Convers. Manage.* 52 (2011) 431–436.
- [13] R. Dev, G.N. Tiwari, Characteristic equation of a passive solar still, *Desalination* 245 (2009) 246–265.
- [14] O.O. Badran, Experimental study of the enhancement parameters on a single slope solar still productivity, *Desalination* 209 (2007) 136–143.
- [15] M. Afrand, A. Behzadmehr, A. Karimipour, A Numerical Simulation of Solar Distillation for Installation in Chabahar-Iran, *Eng. Technol.* 47 (2010) 515–520.
- [16] I. Al-Hayek, O.O. Badran, The effect of using different designs of solar stills on water distillation, *Desalination* 169 (2004) 121–127.
- [17] G.N. Tiwari, V. Dimri, A. Chel, Parametric study of an active and passive solar distillation system: Energy and exergy analysis, *Desalination* 242 (2009) 1–18.
- [18] P.K. Abdenacer, S. Nafila, Impact of temperature difference (water-solar collector) on solar-still global efficiency, *Desalination* 209 (2007) 298–305.
- [19] M. Luo, R. Gupta, J. Frechette, Modulating contact angle hysteresis to direct fluid droplets along a homogenous surface, *ACS Appl. Mater. Interf.* 4 (2)(2012) 890–896.
- [20] P.I. Cooper, Digital simulation of transient solar still processes, *Solar Energy* 12 (1969) 313–331.
- [21] S.H. Soliman, Effect of wind on solar distillation, *Solar Energy* 13 (1972) 403–415.
- [22] A.K. Rajvanshi, Effect of various dyes on solar distillation, *Solar Energy* 27 (1981) 51–65.
- [23] H.P. Garg, H.S. Mann, Effect of climatic, operational and design parameters on the year-round performance of single-sloped and double-sloped stills under Indian arid zone conditions, *Solar Energy* 18 (1976) 159–164.
- [24] K.G.T. Hollands, The regeneration of lithium chloride brine in a solar still for use in solar air conditioning, *Solar Energy* 7 (1963) 39–43.
- [25] H. Yeh, L. Chen, Basin-type solar distillation with air flow through the still, *Energy* 10 (1985) 1237–1241.
- [26] H. Yeh, L. Chen, The effects of climatic, design and operational parameters on performance of wick-type solar stills, *Energy Convers. Manage.* 26 (1986) 175–180.
- [27] J.A. Eibling, S.G. Talbert, G.O.G. Lof, Solar stills for community use—Digest of technology, *Solar Energy* 13 (1971) 263–276.
- [28] A.A. El-Sebaai, Effect of wind speed on active and passive solar stills, *Energy Convers. Manage.* 45 (2004) 1187–1204.
- [29] A.A. El-Sebaai, On effect of wind speed on passive solar still performance based on inner/outer surface temperatures of the glass cover, *Energy* 36 (2011) 4943–4949.